A Non-linear Diffeomorphic Framework for Prostate Multimodal Registration

Jhimli Mitra*†, Zoltan Kato‡, Robert Martí†, Arnau Oliver†, Xavier Lladó†,
Soumya Ghose*†, Joan C. Vilanova§ and Fabrice Meriaudeau*
*Le2i-UMR CNRS 5158, Université de Bourgogne, Le Creusot, France
Email: {jhimli.mitra,fabrice.meriaudeau,soumya.ghose}@u-bourgogne.fr
†Computer Vision and Robotics Group, Universitat de Girona, Girona, Spain
Email: {jmitra,marly,aoliver,llado}@eia.udg.edu
‡Department of Image Processing and Computer Graphics, University of Szeged, Szeged, Hungary
Email: kato@inf.u-szeged.hu
§Girona Magnetic Resonance Center, Girona, Spain

***Abstract*—This paper presents a novel method for non-rigid registration of prostate multimodal images based on a non-linear framework. The parametric estimation of the non-linear diffeomorphism between the 2D fixed and moving images has its basis in solving a set of non-linear equations of thin-plate splines. The regularized bending energy of the thin-plate splines along with the localization error of established correspondences is jointly minimized with the fixed and transformed image difference; where, the transformed image is represented by the set of non-linear equations defined over the moving image. The traditional thin-plate splines with established correspondences may provide good registration of the anatomical targets inside the prostate but may fail to provide improved contour registration. On the contrary, the proposed framework maintains the accuracy of registration in terms of overlap due to the non-linear thin-plate spline functions while also producing smooth deformations of the anatomical structures inside the prostate as a result of established corrspondences. The registration accuracies of the proposed method are evaluated in 20 pairs of prostate mid-gland ultrasound and magnetic resonance images in terms of Dice similarity coefficient with an average of 0.982 ± 0.004, average 95% Hausdorff distance of 1.54 ± 0.46 mm and mean target registration and target localization errors of 1.90 ± 1.27 mm and 0.15 ± 0.12 mm respectively.**

I. Introduction

Prostate cancer in human male has been a major concern in Europe since the last twenty years. A person with increased Prostate Specific Antigen (PSA) is advised for a prostate biopsy for further histological analysis of the prostate tissue. The needle biopsy of the prostate is often performed using interventional Transrectal Ultrasound (TRUS). The TRUS images do not provide enough soft tissue contrast and therefore $10 - 12$ samples are strategically extracted from the prostate region [1]. However, this multicore biopsy strategy may also increase the number of re-biopsies required. Magnetic Resonance Imaging (MRI) has a negative predictive value $\geq 95\%$ for significant cancer and therefore may reduce the number of re-biopsies while at the same time provide more useful information for those who are sent for biopsy [2]. Therefore, fusion of pre-biopsy MR images onto interventional TRUS images might increase the overall biopsy accuracy [3], [4]. Fig. 1 shows the TRUS and the corresponding MR slices of a prostate where the encircled areas mark a tumor that is almost iso-echoic in TRUS but can be seen with better contrast in the MR image.

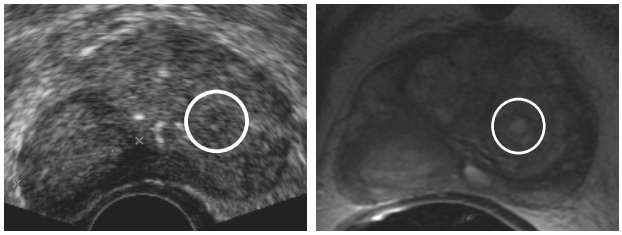


Fig. 1. TRUS and corresponding MR images of a prostate. (a) The encircled area shows a tumor iso-echoic with the normal prostate tissue in TRUS image, (b) the encircled area shows the tumor in MR image with a different contrast than the normal prostate tissue.

The prostate of the same patient may undergo deformations during the TRUS or MRI procedures due to full bladder or bowel or gas inside the rectum, altered patient positions on the couch and inflation of the endorectal balloon inside the rectum containing the MR coil. In order to cope with these deformations, non-rigid registration methods are applied for prostate multimodal registration [5]–[7]. Spline-based deformations have been commonly used to register prostate multimodal images. Prostate MR volumes were warped using thin-plate splines (TPS) by Fei et al. [8] where the prostate centroid displacement was observed to be 0.6 mm. Oguro et al. [9] registered pre- and intra-operative MR images for prostate brachytherapy. The Dice Similarity Coefficient (DSC) value for the total gland was reported as 0.91 and the fiducial registration error was 2.3 ± 1.8 mm respectively. TRUS and MR multimodal registration for interventional biopsy was investigated by Mitra et al. [10]. The method was based on TPS with automatic point correspondences generated with an average DSC of 0.97 ± 0.01 for 4 patient datasets.

Bookstein [11] originally proposed the interpolating TPS that involves the establishment of a set of point correspondences on a pair of images. However, these sets of correspondences are prone to error in real applications and therefore

Rohr et al. [12] extended the bending energy of TPS to approximation and regularization by introducing the correspondence localization error. Nevertheless, all these methods are dependant on a set of point correspondences on the pair of images to be registered. On the contrary, Nemeth et al. [13], [14] proposed a class of non-rigid registration that does not require explicit point correspondences and instead registers binary images solving a set of non-linear equations to either recover the plane projective transformation or to obtain the parameters of polynomial deformation between the images.

In this work, we have exploited the advantages of having point correspondences to better localize the anatomical structures inside the prostate that are clinically meaningful, along with the non-linear transformation that produces smooth deformations to provide maximum overlap of the prostate in the fixed and the transformed images. Therefore, we have extended the work of Nemeth et al. [13], [14] by constraining the solution of the set of non-linear TPS equations with the regularized bending energy and the quadratic approximation term of TPS to obtain the TPS transformation parameters. The point correspondences for the set of prostate images are established using the method in [10] however, the number of point correspondences are fixed in our case. The proposed method validated on 20 pairs of prostate TRUS and MR images shows a low average Target Registration Error (TRE) of 1.90 ± 1.27 mm and an average DSC value of 0.982 ± 0.004. The remaining of the paper is organized as follows. Section II explains the proposed method, section III provides the results and discussions with section IV drawing the conclusions.

II. Methodology

The point correspondences are established in the fixed and moving prostate images and then the transformation parameters are obtained using a non-linear framework based on TPS. This section consists of two parts, the first part provides a brief discussion on the method of selecting point correspondences in the fixed and moving images. While, the second part provides a discussion on the non-linear framework of TPS.

A. Point correspondences

The method used for selecting the point correspondences is directly based on the method of Mitra et al. [10]. However, the number of levels of correspondences is fixed to the 3rd level i.e. 32 point correspondences on the prostate contours. According to the sizes of the prostate in the TRUS and MR images, this number of correspondences on the contours was found to be sufficient.

The method assumes that the prostate is initially segmented in both the fixed and moving images and establishing the point correspondences begins by first translating the principal axes of the fixed prostate image on the moving image. The process thereafter may be summarized as follows: Let p_i, where, $i = 1, ..., n$ and $n = 4$ for level $r = 0$, represent the four intersections of the principal axes with the prostate contour. With the final level $R = 3$, the algorithm is as follows:

1) Level $r = 0$.
2) Loop while $r <= R$.
3) $r = r + 1$.
4) Generate midpoint q_i between p_i and p_{i+1} as $(p_i + p_{i+1})/2$.
5) Find a point d_i on the contour between p_i and p_{i+1} such that $slope(p_i, p_{i+1}) \times slope(d_i, q_i) = -1$.
6) (p_i, d_i, p_{i+1}) comprise the triangulated region of the prostate between p_i and p_{i+1}.
7) Repeat steps 4-6 until $p_i = p_n$ and $p_{i+1} = p_1$.
8) If $r <= R$, then update $n = 2n$ and save $p_1, d_1, p_2, ..., p_{n-1}, d_{n-1}, p_n, d_n$ as new p_i with $i = 1, ..., n$ and repeat from Step 3. Else, end the loop.

Due to the fact that the points on the prostate contours are not enough for a smooth deformation, certain points inside the prostate are also considered. These are the centroid c and the 4 points z_i that are generated inside the prostate as the mid-points between the points q_i generated at level $r = 1$ and the centroids. It is to be noted that this approach is slightly different from that of Mitra et al. [10] as the inside points taken by them were the q_i. However, we noticed that if the lower part of the prostate has higher concavity then either of these internal points may fall outside the prostate boundary and therefore will hinder in obtaining a proper deformation field. Fig. 2 shows the points generated for the 1st level and the 37 final correspondences at the 3rd level on the fixed and moving prostate contour images respectively.

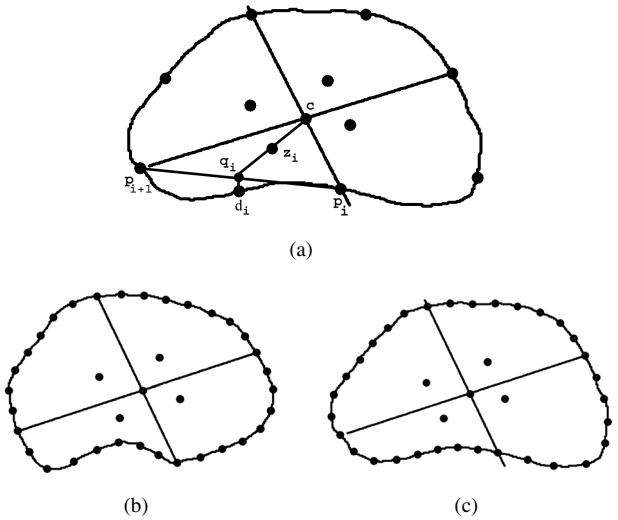


Fig. 2. Point correspondences example. (a) Points generated for 1st level, (b) fixed image points at 3rd level and (c) moving image points at 3rd level.

B. Non-linear Diffeomorphism

To align a pair of binary shapes, let us consider the moving and the fixed images be $\mathrm{x} = [x_1, x_2] \in \mathbb{R}^2$ and $\mathrm{y} = [y_1, y_2] \in \mathbb{R}^2$ respectively, such that there exists a bijective transformation $\varphi(.)$ and $\varphi^{-1}(.)$ between the images as

$$\mathrm{y} = \varphi(\mathrm{x}) \Leftrightarrow \mathrm{x} = \varphi^{-1}(\mathrm{y}). \quad (1)$$

The deformation field $\varphi(.)$ can be decomposed for x- and y-coordinates respectively as $\varphi(\mathrm{x}) = [\varphi_1(\mathrm{x}), \varphi_2(\mathrm{x})]$, where $\varphi_1, \varphi_2 : \mathbb{R}^2 \rightarrow \mathbb{R}$. If explicit point correspondences are not established then the diffeomorphism is obtained by integrating over the foreground pixels of the fixed and moving image domains I_f and I_m respectively [13]:

$$\int_{I_f} \mathrm{y} d\mathrm{y} = \int_{I_m} \varphi(\mathrm{x}) \left| J_\varphi(\mathrm{x}) \right| d\mathrm{x}, \tag{2}$$

where the integral transformation $\mathrm{y} = \varphi(\mathrm{x})$ and $d\mathrm{y} = |J_\varphi(\mathrm{x})|\, d\mathrm{x}$ with $|J_\varphi| : \mathbb{R}^2 \rightarrow \mathbb{R}$ being the Jacobian of the transformation at each foreground pixel of the moving image.

It is to be noted that the identity relation of (1) is only valid under the influence of a set of non-linear functions $\omega_k(.) : \mathbb{R}^2 \rightarrow \mathbb{R}$ where, $k = 1, \ldots, l$ acting on both sides of (2) as

$$\int_{I_f} \omega_k(\mathrm{y}) d\mathrm{y} = \int_{I_m} \omega_k\big(\varphi(\mathrm{x})\big) \left| J_\varphi(\mathrm{x}) \right| d\mathrm{x}. \tag{3}$$

Therefore to estimate the parameters of the transformation, the number of non-linear functions l, must be more than the number of parameters to generate a set of linearly independent equations.

In this work, the underlying transformation is considered to be the radial-basis function of TPS where the foreground pixels of the moving image deform under the influence of the control points $p_i : \mathbb{R}^2$ established by the method of section II-A. The TPS transformation is given as

$$\varphi_v(\mathrm{x}) = a_{v1}x_1 + a_{v2}x_2 + a_{v3} + \sum_{i=1}^{n} w_{iv} U(\|p_i - \mathrm{x}\|), \tag{4}$$

where, a_{vu} are the 6 affine parameters, w_{iv} are the TPS weight parameters for the control points with $i = 1, \ldots n$, $v = 1, 2$, $u = 1, 2, 3$, $U : \mathbb{R} \rightarrow \mathbb{R}$ is the radial-basis function as $U(r) = r^2 \log r^2$ and $\|.\|$ is the Euclidean norm. The additional constraints for the TPS interpolation are that the sum of the weights applied to the plate as well as moments with respect to both axes should be 0 and are given as

$$\sum_{i=1}^{n} w_{iv} = 0 \quad \text{and} \quad \sum_{i=1}^{n} p_{iv} w_{iv} = 0. \tag{5}$$

However, the transformation of (4) when replaced in (3) will only consider the point set on the moving image under the influence of which the image deforms to match the fixed image, therefore, the gray-level deformations of the regions inside the prostate may not be meaningful for clinical applications. The correspondences p_i, established across the fixed and moving image domains as $p_i^f = \left[p_{y_{i1}}^f, p_{y_{i2}}^f\right]$ and $p_i^m = \left[p_{x_{i1}}^m, p_{x_{i2}}^m\right]$, $i = 1, \ldots, n$ respectively, play an important role in constraining these deformations. We introduce the bending energy of the correspondences across the fixed and moving images as an additional constraint to solve the set of equations in (3) and is given by

$$E_{TPS} = \int_i \int_i \left(\frac{\partial^2 \zeta}{\partial {p_{x_{i1}}^m}^2} \right)^2 + 2 \left(\frac{\partial^2 \zeta}{\partial p_{x_{i1}}^m \partial p_{x_{i2}}^m} \right)^2 + \left(\frac{\partial^2 \zeta}{\partial {p_{x_{i2}}^m}^2} \right)^2 \partial p_{x_{i1}}^m \partial p_{x_{i2}}^m \tag{6}$$

where, $\zeta : \mathbb{R}^2 \rightarrow \mathbb{R}^2$, $\zeta = [\zeta_1(p_i^m), \zeta_2(p_i^m)]$ is the transformation of the point correspondences established on the moving image to match with those of the fixed image.

$$\zeta = \zeta_v(p_i^m) = a_{v1}p_{x_{i1}}^m + a_{v2}p_{x_{i2}}^m + a_{v3} + \sum_{i=1}^{n} w_{iv} U(p_i^m - p_i^f) \tag{7}$$

with $v = 1, 2$. Finally, the equation acting as a constraint is the regularized TPS bending energy with the quadratic approximation term that considers the correspondence localization error is

$$\frac{1}{n} \sum_{i=1}^{n} \frac{\left\| p_i^f - \zeta(p_i^m) \right\|^2}{\sigma_i^2} + \lambda E_{TPS} = 0, \tag{8}$$

where, σ_i^2s are the variances of the correspondences between the fixed and moving images, λ is a regularization factor set empirically, $\zeta(p_i^m)$ is obtained from (7) and E_{TPS} from (6).

The adopted set of non-linear functions are the power functions as proposed in [14] as

$$\omega_k(\mathrm{x}) = x_1^{a_k} x_2^{b_k}, \tag{9}$$

with $(a_k, b_k) \in \big\langle (0,0), (1,0), (0,1), (1,1), (2,0), (0,2), (2,1), (1,2), (2,2), (3,0), (0,3), (3,1), (1,3), (3,2), (2,3), (3,3), \ldots, (9,9) \big\rangle$. The total number of parameters to be estimated is 80 that comprises of 6 affine and 37×2 TPS weight parameters for 37 correspondences. Therefore, 100 linearly independent equations are generated using the power set of $\omega_k(.)$ functions with 4 equations for (5) and one for (6). The solution to the set of non-linear equations is obtained using the *Levenberg-Marquardt* (LM) algorithm [15]. It is to be noted that the foreground pixels of the moving and fixed images are normalized within a unit square $[-0.5, 0.5] \times [-0.5, 0.5]$ so that the shape centers become the origins.

III. Results and Discussions

The proposed registration method is evaluated using prostate mid-gland images of TRUS and MR for 20 patients. The average size of the images being 249×199 pixels. The axial MRI acquisition of the prostate was done using a GE Signa HDxt 1.5 Tesla machine and the axial TRUS images were acquired using a 6.5MHz side-firing probe and SIEMENS Allegra machine. The MR slice from the axial MR volume that closely corresponds to the axial TRUS mid-gland prostate image is manually chosen by an expert. However, the slice correspondence will be eventually established in an automatic manner with the use of an electromagnetic tracker [4]. In

TABLE I

A COMPARISON OF REGISTRATION ACCURACIES OF THE TPS REGISTRATION [10] AND THE PROPOSED NON-LINEAR TPS FRAMEWORK. μ IS THE MEAN AND σ IS THE STANDARD DEVIATION OF THE MEASURES.

Patient#	***TPS [10]***				***Proposed Method***			
	DSC	HD (mm)	TRE (mm)	TLE (mm)	DSC	HD (mm)	TRE (mm)	TLE (mm)
1	0.971	1.84	9.36	0.22	0.971	2.08	2.30	0.28
2	0.957	2.32	3.98	0.10	0.983	0.94	1.32	0.07
3	0.974	2.09	7.92	0.13	0.985	1.40	3.14	0.09
4	0.982	1.40	5.21	0.49	0.986	1.16	1.07	0.54
5	0.972	2.35	2.11	0.07	0.979	1.32	0.94	0.08
6	0.979	2.32	1.17	0.05	0.975	1.82	0.80	0.03
7	0.977	2.61	4.43	0.12	0.984	1.64	4.49	0.10
8	0.978	2.96	3.57	0.05	0.983	1.56	1.53	0.11
9	0.978	2.39	2.70	0.46	0.980	2.90	2.15	0.24
10	0.972	1.98	6.09	0.04	0.985	1.47	3.85	0.03
11	0.972	2.22	2.98	0.12	0.982	1.87	1.56	0.07
12	0.971	5.00	2.44	0.12	0.981	1.40	0.39	0.21
13	0.980	1.84	3.06	0.07	0.985	1.30	4.03	0.07
14	0.986	0.82	1.75	0.07	0.987	1.04	0.25	0.05
15	0.968	2.22	2.29	0.07	0.979	1.64	1.78	0.07
16	0.970	2.71	1.86	0.07	0.985	1.30	2.17	0.10
17	0.982	1.04	0.18	0.32	0.982	1.10	1.26	0.27
18	0.982	1.64	0.91	0.26	0.981	1.40	1.34	0.23
19	0.983	1.66	1.47	0.23	0.979	2.14	3.31	0.12
20	0.973	2.08	3.11	0.30	0.980	1.30	0.30	0.19
μ	**0.975**	**2.17**	**3.33**	**0.17**	**0.982**	**1.54**	**1.90**	**0.15**
σ	**0.007**	**0.85**	**2.33**	**0.14**	**0.004**	**0.46**	**1.27**	**0.12**

our experiments, the prostate from the TRUS and MR images are segmented manually by an expert so that automatic segmentation errors are not propagated in the evaluation of true registration accuracies. The TRUS slice is the fixed image and the respective MR slice is the moving image for all the experiments. The registration accuracies are evaluated in terms of DSC, 95% Hausdorff Distance (HD), TRE and Target Localization Error (TLE).

DSC is a measure of overlap of the same foreground labels (E) between the transformed moving image ($M(E)$) and the fixed image ($F(E)$) and is given by

$$\text{DSC} = \frac{2(M(E) \cap F(E))}{M(E) + F(E)}. \tag{10}$$

Given a set of finite points $B1 = \{b1_1, \ldots, b1_p\}$ and $B2 = \{b2_1, \ldots, b2_q\}$, the Hausdorff distance between the point sets is defined by

$$HD(B1, B2) = \max(h(B1, B2), h(B2, B1)) \tag{11}$$

$$\text{where,} \quad h(B1, B2) = \max_{b1 \in B1} (\min_{b2 \in B2} \|b1 - b2\|) \tag{12}$$

A target is an anatomical landmark in the patient's body and is normally the centroid of a lesion, tumor, gland, etc. that is not used to compute the transformation of the moving image to the fixed image. TRE is the root mean square distance of such homologous targets tp_i^m and tp_i^f, $i = 1, 2, \cdots, N$ on the moving and the fixed images respectively and is given by

$$\text{TRE} = \frac{1}{N} \sqrt{\sum_{i=1}^{N} (\varphi(tp_i^m) - tq_i^f)^2}, \tag{13}$$

where, $\varphi(.)$ is the transformation of the moving image. The targets used in our experiments are primarily the centroids of lesions and tumors in the central gland, the prostatic urethra, sometimes the centroids of tumors in the peripheral region and the centroid of the central gland in few cases where lesions or other homologous structures are not visible in TRUS as in the corresponding MRI. The repeatability error in the localization of the targets is given as the TLE computed from the centroids of manually selected regions from 5 independent trials by an experienced radiologist.

The proposed registration method is compared with the method in [10]. Table I shows the results of 20 patients with the DSC, HD, TRE and TLE values for both the registration methods. It is to be noted from Table I that the contour overlap measures in terms of DSC and HD are generally higher for our proposed method. The mean DSC and mean HD for the proposed method are 0.982 ± 0.004 and 1.54 ± 0.46 mm respectively and that of TPS [10] are 0.975 ± 0.007 and 2.17 ± 0.85 mm respectively. This shows that our method performs significantly better than traditional TPS and has high statistical significance for DSC and HD measures using two-tailed Student's *t*-test $p < 0.001$ and $p < 0.006$ respectively. The DSC values are transformed using an *arcsin* transform so that the resulting values follow a normal distribution which is a necessary condition to perform Student's *t*-test. As observed from the table that the TRE values for 14 out of 20 patients are better using our method and the mean TRE is 1.90 ± 1.27 mm. However, due to larger standard deviations this value has statistical significance of *t*-test $p < 0.02$ when compared to TPS [10]. The low mean TLE values of 0.15 ± 0.12 mm and 0.17 ± 0.14 mm for our method and TPS [10]

respectively indicate that repeated independent identification of local structures inside the prostate has been consistent.

Fig. 3 shows some registration results of the proposed method along with the results obtained using TPS [10] on our datasets. The method in [10] does not require the prostates to be segmented to perform the registration apart from establishing the correspondences on the contours and therefore, the results are shown on non-segmented prostates. However, our proposed method requires the registration to be performed on the segmented prostates. It is observed that smoother contours are obtained for patients 2, 3, 6, 7, 12, 13 (rows 1, 2, 3, 4, 8 and, 9 respectively) with our method (columns $5-6$) than with TPS [10] (columns $3-4$). The small structure at the base of the central gland of the prostate identified as the prostatic urethra in the MR images (column 2) for patients 6 and 12 (rows 3 and 8 respectively) are seen to be properly deformed when our proposed method is used (column $5-6$) compared to the traditional TPS method (column $3-4$). Similarly, the prostate central glands overlap more accurately after deformation with that of the respective TRUS images (column 1) using our method (column 6) for patients 2, 3, 7, 11 and, 12 (rows 1, 2, 4, 7 and, 8 respectively) than the other method (column 4).

Our method is implemented on MATLAB 2009(b) on an Intel Core2Duo 1.66 GHz processor with 2 GB RAM. The average time required for our proposed method from control point genereration to the LM optimization for 20 cases is 320.79 ± 76.01 secs with the lowest and higest computation times being 152.74 secs and 488.44 secs respectively. The algorithm being highly dependent on the size of the images and considering its unoptimized implementation in MATLAB, a speed-up of computation time is possible by GPU programming.

IV. Conclusions and Future Works

A new non-linear diffeomorphic framework with TPS being the underlying transformation has been proposed to register prostate multimodal images. The bijectivity of the diffeomorphism is maintained by integrating over a set of non-linear functions for both the fixed and transformed moving images. Added to the constraints for the TPS deformation of the moving image, the bending energy of the point correspondences established between the fixed and moving images and their localization error are also introduced into the system of non-linear equations. This additional constraint ensures regularized deformations of the local anatomical structures inside the prostate that are meaningful for clinical interventions like prostate biopsy.

The extension of the non-linear TPS framework for 3D prostate volume registration is possible. However, a symmetric method to generate point correspondences in the respective volumes needs to be developed. The TRUS-MR slice correspondences chosen manually in our experiment can be done automatically with the use of an electromagnetic tracker attached to the TRUS probe that will provide the z-coordinate position during the needle-biopsy. The algorithm can be parallelized if programmed on GPU and therefore, may be useful for real-time multimodal fusion of prostate images during biopsy.

Acknowledgments

This research is financially supported by the PROSCAN project VALTEC 08-1-0039 of Generalitat de Catalunya, Spain, the Conseil Régional de Bourgogne, France, and the grant CNK80370 of the National Office for Research and Technology (NKTH) & Hungarian Scientific Research Fund (OTKA); the EU and by the European Regional Development Fund within the projects TAMOP-4.2.2/08/1/2008-0008 and TAMOP-4.2.1/B-09/1/KONV-2010-0005.

References

[1] C. R. Porter, C. O'Donnell, E. D. Crawford, E. J. Gamito, J. Kim, and A. Tewari, "Predicting the outcome of the random prostate biopsy," Department of Urology, State University of New York, Stony Brook,NY., Tech. Rep., http://www.cancernews.com/data/Article/230.asp, accessed [7th Jun, 2010].

[2] J. C. Vilanova, C. Barceló-Vidal, J. Comet, M. Boada, J. Barceló, J. Ferrer, and J. Albanell, "Usefulness of prebiopsy multi-functional and morphologic MRI combined with the free-to-total PSA ratio in the detection of prostate cancer," *American Journal of Roentgenology*, vol. 196, no. 6, pp. W715–W722, 2011.

[3] I. Kaplan, N. E. Oldenburg, P. Meskell, M. Blake, P. Church, and E. J. Holupka, "Real time MRI-ultrasound image guided stereotactic prostate biopsy," *Magnetic Resonance Imaging*, vol. 20, pp. 295–299, 2002.

[4] S. Xu, J. Kruecker, B. Turkbey, N. Glossop, A. K. Singh, P. Choyke, P. Pinto, and B. J. Wood, "Real-time MRI-TRUS fusion for guidance of targeted prostate biopsies," *Computer Aided Surgery*, vol. 13, no. 5, pp. 255–264, 2008.

[5] C. Reynier, J. Troccaz, P. Fourneret, A. Dusserre, C. Gay-Jeune, J.-L. Descotes, M. Bolla, and J.-Y. Giraud, "MRI/TRUS data fusion for prostate brachytherapy. preliminary results," *Medical Physics*, vol. 31, no. 6, pp. 1568–1575, 2004.

[6] R. Narayanan, J. Kurhanewicz, K. Shinohara, E. D. Crawford, A. Simoneau, and J. S. Suri, "MRI-ultrasound registration for targeted prostate biopsy," in *Proc. of IEEE Intl. Symposium on Biomedical Imaging: From Nano to Macro (ISBI'2009)*, Boston, MA, Jun./Jul. 2009, pp. 991–994.

[7] A. du Bois d'Aische, M. D. Craene, S. Haker, N. Weisenfeld, C. Tempany, B. Macq, and S. K. Warfield, "Improved non-rigid registration of prostate MRI," in *Proc. of MICCAI*, vol. LNCS 3216, Rennes, France, Sep. 2004, pp. 845–852.

[8] B. W. Fei, C. Kemper, and D. L. Wilson, "A comparative study of warping and rigid body registration for the prostate and pelvic MR volumes," *Computerized Medical Imaging and Graphics*, vol. 27, pp. 267–281, 2003.

[9] S. Oguro, J. Tokuda, H. Elhawary, S. Haker, R. Kikinis, C. M. Tempany, and N. Hata, "MRI signal intensity based B-spline nonrigid registration for pre- and intraoperative imaging during prostate brachytherapy." *Magnetic Resonance Imaging*, vol. 30, no. 5, pp. 1052–1058, 2009.

[10] J. Mitra, A. Oliver, R. Martí, X. Lladó, J. C. Vilanova, and F. Meriaudeau, "Multimodal prostate registration using thin-plate splines from automatic correspondences," in *Proc. of Intl. Conference on Digital Image Computing:Techniques and Applications (DICTA'10)*, Sydney, Australia, Dec. 2010, pp. 587–592.

[11] F. Bookstein, *Morphometric Tools for Landmark Data: Geometry and Biology*. Cambridge, UK: Cambridge University Press, 1991.

[12] K. Rohr, H. S. Stiehl, R. Sprengel, T. M. Buzug, J. Weese, and M. H. Kuhn, "Landmark-based elastic registration using approximating thin-plate splines," *IEEE Transactions on Pattern Analysis and Machine Intelligence*, vol. 20, no. 6, pp. 526–534, June 2001.

[13] J. Nemeth, C. Domokos, and Z. Kato, "Recovering planar homographies between 2D shapes," in *Proc. IEEE International Conference on Computer Vision (ICCV'09)*, Kyoto, Japan, Sep. 2009, pp. 2170–2176.

[14] ——, "Nonlinear registration of binary shapes," in *Proc. IEEE International Conference on Image Processing (ICIP'09)*, Cairo, Egypt, Nov. 2009, pp. 1001–1004.

[15] D. W. Marquardt, "An algorithm for least-squares estimation of nonlinear parameters," *SIAM Journal on Applied Mathematics*, vol. 11, no. 2, pp. 434–441, 1963.

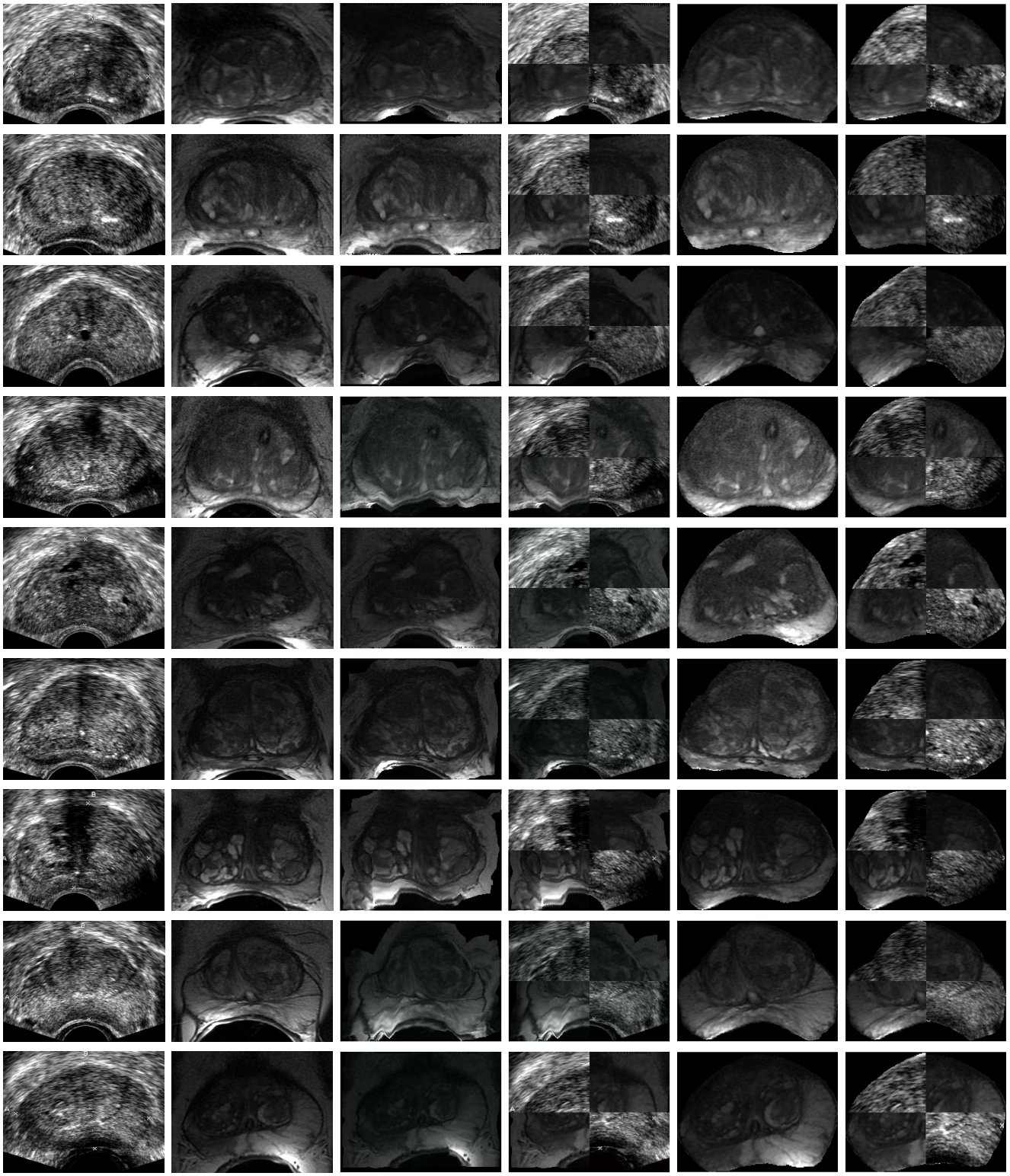


Fig. 3. Qualitative registration results for patients 2, 3, 6, 7, 8, 10, 11, 12 and 15 in rows. Column 1 shows the fixed TRUS images, column 2 shows the moving MR images, columns $3-4$ show the registration results in terms of transformed MR images and checker-board using TPS [10] and columns $5-6$ using our proposed method.